J. Fluid Mech. (1997), *vol.* 332, *pp.* 121–139

Copyright © 1997 Cambridge University Press

On the formation and propagation of vortex rings and pairs of vortex rings

By S. L. WAKELIN AND N. RILEY
School of Mathematics, University of East Anglia, Norwich NR4 7TJ, UK

(Received 30 November 1995 and in revised form 7 August 1996)

Axisymmetric high-Reynolds-number laminar flows are simulated numerically. In particular, we consider the formation and propagation of single vortex rings from a circular orifice in a plane boundary, and pairs of vortex rings from a circular annulus in a plane boundary. During formation, single rings grow within an essentially potential flow, as in the similarity theory of Pullin (1979). When released they are shown to propagate in an almost inviscid manner, as described by Saffman (1970). Pairs of vortex rings, formed at a circular annulus, have been studied by Weidman & Riley (1993), both experimentally and computationally. They conclude from their observations that the behaviour of the rings depends primarily upon two parameters, namely the impulse applied to the fluid, during ring formation, and the gap width of the annulus. The results we present in this paper confirm the dependence of the flow on these parameters.

1. Introduction

The motivation for the present investigation is largely provided by the work of Weidman & Riley (1993). They presented the results from an experiment, with water as the working fluid, in which the fluid was forced by a piston through a circular annulus, with the gap width relatively small compared to its diameter. Vortex rings were formed at the edges of the annulus, with circulation of opposite sign, which propagated into the fluid exhibiting a variety of behaviour. A numerical simulation, based upon the Navier–Stokes equations, was in qualitative accord with observation. In a subsequent paper Riley (1993) examined further, by numerical simulation, a wider variety of behaviour exhibited by pairs of vortex rings. At high Reynolds numbers it was conjectured by Riley that these interactions between the vortex rings are largely inviscid phenomena. With that in mind, Wakelin & Riley (1996) have used two inviscid models, based on both a thin-ring theory and a contour-dynamic approach, to study the behaviour of pairs of vortex rings. The results reflect, satisfactorily, the viscous-flow behaviour.

None of the computational efforts mentioned above address the formation of the vortex rings. In the viscous calculations the not unreasonable assumption was made that the vortex rings when formed, at the end of the piston stroke, would have thin, axisymmetric cores, which were then modelled by a viscous line vortex (Lamb 1932). The circulation about the outer ring Γ_0, and hence the ring Reynolds number Γ_0/ν, was determined from the observed timescale of a particular experiment, and the circulation about the inner ring was fixed by seeking the best agreement with experiment, which was highly satisfactory. In this paper we are concerned not only with the propagation of vortex rings, but also their formation. As well as pairs of rings we consider the formation and propagation of single rings.

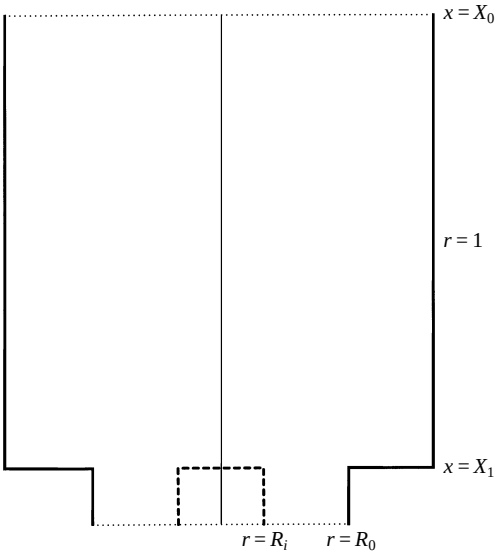

FIGURE 1. Definition sketch. For pairs of vortex rings the inner cylinder $r \leqslant R_i$, $x \leqslant X_1$ is introduced.

Figure 1 shows the configuration within which we generate, and study, the vortex rings. A circular cylindrical tube is open at one end. At the other it contracts abruptly. Within it may be a smaller circular cylinder, so that when fluid is forced from the lower end of the narrow tube a vortex ring forms at the lip where the tube widens or, correspondingly, a pair of vortex rings when the inner tube is present. The numerical method for solution of the unsteady Navier–Stokes equations is an ADI method, based on that described by Weidman & Riley (1993). The main differences are in the boundary conditions at the open, upper end of the cylinder, the inflow conditions at the lower end and the accommodation of the singular behaviour at the corners of the expansion, and the inner cylinder, when present.

The first results we obtain, in §4, are for the formation of single rings, at the corner of the expansion when the inner cylinder is absent. Although we are not able to make a direct comparison with Pullin's (1979) similarity theory, our results are not inconsistent with it. And furthermore, we confirm that the basis for his theory, namely a vortex ring growing within an initial potential flow, is sound. With the vortex ring formed, and propagating freely with its self-induced velocity, we see that its speed is almost constant as in an inviscid fluid. With that in mind we compare the shape of the cross-section of the ring with an inviscid ring that has the same speed, radius and circulation at a given instant from the family of Norbury (1973) rings. Unsurprisingly they are very similar. By considering different cases we show that the flow characteristics are largely independent of Reynolds number, but are significantly influenced by the impulse of the initial inlet flow. The observation of weak dependence upon Reynolds number is reinforced by a comparison with Saffman's (1970) result for the velocity of viscous vortex rings at high Reynolds number.

With the inner cylinder in place, see figure 1, we are able to generate pairs of vortex rings. Although our configuration from which these are formed is much simpler than that in the experiments of Weidman & Riley (1993), we do expect to observe behaviour similar to that in the experiments, and indeed we do. In particular we confirm that the annular gap width and impulse of the inlet flow are the crucial parameters that

determine the flow characteristics. The axisymmetric flows with which we are concerned fall into three main categories. If, on formation, the inner ring is sufficiently strong it separates from the outer ring, and propagates back towards its origins. If it is sufficiently weak the interaction between the rings results in it being pushed ahead of, and then outside, the outer ring. Between these is the delicate balance that can result in a quasi-steadily propagating structure, named a vortex-ring pair by Weidman & Riley, in which the two vortex rings propagate in an almost co-planar manner. All three cases have been observed in the experiments, and created in the simulations described in §4. The flow visualizations of Weidman & Riley (1993) yielded little information about the flow structure beyond the vortex ring trajectories. Coloured dye was entrained into the vortex rings during formation and a residual blob at the centre of the ring core allowed it to be traced. We also present trajectories of the vortex rings for ease of illustration. But our simulations allow further insight into the flow structure. Our results show, in particular, that the inner ring is always the 'junior partner' in the sense that it is slightly weaker on formation, and in all cases decays more rapidly than the outer when in its proximity, to the extent that it almost loses its identity completely in those situations where close contact is maintained throughout most of the interaction. The flow structures that we predict also raise questions about the role of the initial conditions used in the numerical simulations of Weidman & Riley.

2. The governing equations

The governing equations are the Navier–Stokes equations for an incompressible fluid. From these we have Helmholtz's equations for the vorticity $\boldsymbol{\omega}'$ as

$$\frac{\partial \boldsymbol{\omega}'}{\partial t'} - \boldsymbol{\nabla} \wedge (\boldsymbol{v}' \wedge \boldsymbol{\omega}') = -\nu \boldsymbol{\nabla} \wedge \boldsymbol{\nabla} \wedge \boldsymbol{\omega}' \tag{2.1}$$

together with

$$\boldsymbol{\nabla} \cdot \boldsymbol{v}' = 0, \tag{2.2}$$

where ν is the kinematic viscosity, $\boldsymbol{v}'$ is the velocity, t' is the time and

$$\boldsymbol{\omega}' = \boldsymbol{\nabla} \wedge \boldsymbol{v}'. \tag{2.3}$$

We are concerned with the generation and subsequent motion of axisymmetric vortex rings in a circular cylinder of total length l. At the inflow end the cylinder is of radius a_0, which changes abruptly to a radius $a > a_0$ at a distance l_0 along the cylinder. This results in a convex corner of angle $\pi/2$ in the cylinder wall at which vorticity is shed when fluid is forced through the cylinder. We use cylindrical polar coordinates (r', θ, x'), with the corresponding velocity components (u', v', w'). Let Γ_0 be a typical circulation associated with a ring. The physical variables are made dimensionless with respect to the length a, time a^2/Γ_0, velocity Γ_0/a and vorticity Γ_0/a^2.

We assume that the flow is axisymmetric and that there is no swirl, so that $\boldsymbol{v} = (u, 0, w)$ and $\boldsymbol{\omega} = (0, \zeta, 0)$, where $\zeta = \partial u/\partial x - \partial w/\partial r$. To satisfy (2.2) we introduce a stream function ψ such that

$$u = \frac{1}{r}\frac{\partial \psi}{\partial x}, \quad w = -\frac{1}{r}\frac{\partial \psi}{\partial r}. \tag{2.4}$$

Rather than use the vorticity component ζ we choose to work with a vorticity function defined as

$$\gamma = -r\zeta = r\left(\frac{\partial w}{\partial r} - \frac{\partial u}{\partial x}\right). \tag{2.5}$$

The equations for γ and ψ are given by the θ-component of (2.1) and by (2.2) respectively as

$$\frac{\partial \gamma}{\partial t}+u\frac{\partial \gamma}{\partial r}+w\frac{\partial \gamma}{\partial x}-\frac{2u\gamma}{r}=\frac{1}{Re}\mathrm{D}^2\gamma, \tag{2.6}$$

$$\mathrm{D}^2\psi=-\gamma, \tag{2.7}$$

where

$$\mathrm{D}^2=\frac{\partial^2}{\partial r^2}-\frac{1}{r}\frac{\partial}{\partial r}+\frac{\partial^2}{\partial x^2}$$

and $Re=\Gamma_0/\nu$ is the Reynolds number.

The computational domain is defined as the union of the two regions $0 \leqslant r \leqslant R_0$, $0 \leqslant x < X_1$ and $0 \leqslant r \leqslant 1$, $X_1 \leqslant x \leqslant X_0$, where $R_0=a_0/a$, $X_1=l_0/a$, $X_0=l/a$ and the axis of symmetry lies along $r=0$. On the boundary $x=0$ we introduce an inflow velocity $w_0(r,t)=f(r)\,g(t)$. This allows us to simulate the motion of a piston in the tube, by introducing a spatial variation that consists of a uniform core flanked by a thin boundary-layer region. In all the cases considered the choice of $g(t)$ is such that the ring is well clear of the boundary $x=X_1$ when the inflow ceases. The choice of $f(r)$ is not crucial, as flow conditions at $x=X_1$ are largely independent of it. On $x=X_0$ the relatively unrestrictive condition $\partial u/\partial x=\partial\gamma/\partial x=0$ is adopted; for a discussion of outflow conditions reference may be made to Roache (1972). All other boundaries are impermeable no-slip boundaries at which $u=w=0$, ψ is prescribed and conditions for γ may be derived. Initially, at time $t=0$, all flow variables are zero over the whole domain.

3. The numerical method

Equations (2.6) and (2.7) together with appropriate initial and boundary conditions are solved using finite-difference methods. A uniform grid with nodes at (r_i, x_j) for $i=1, \ldots, m, j=1, \ldots, n$ is used; $\delta r=(m-1)^{-1}$ and $\delta x=X_0(n-1)^{-1}$ are the grid spacings. The grid is formed so that the corner of the boundary at $x=X_1$, $r=R_0$ is located at a grid point, say $R_0=r_I=(I-1)\,\delta r$ and $X_1=x_J=(J-1)\,\delta x$. The values of ψ and γ at each point in the domain, that is, $\psi_{i,j}$ and $\gamma_{i,j}$ for $i=1, \ldots, I$, $j=1, \ldots, J-1$ and $i=1, \ldots, m$, $j=J, \ldots, n$ are determined for $t>0$.

Since (2.6) is parabolic we can march the vorticity function forward in time, with steps of size δt, whilst ensuring that the elliptic equation (2.7) and the boundary conditions are satisfied at each time. At each timestep the values of ψ and γ are known on some sections of the boundary. The remaining boundary values are calculated iteratively during the process to update values of $\gamma_{i,j}$ and $\psi_{i,j}$ inside the domain.

In the finite-difference representations of (2.6) and (2.7) all spatial derivatives are represented by second-order centred differences. Given values of $\gamma_{i,j}$ at each grid point, (2.7) is solved iteratively for $\psi_{i,j}$ using successive over-relaxation. The vorticity equation (2.6) is integrated in time using an alternating-direction implicit (ADI) method as described, for example, by Weidman & Riley (1993). After each ADI step it is necessary to update values of the vorticity function γ on the whole boundary, except for the symmetry line $r=0$, and values of the stream function ψ on the outflow boundary. The vorticity function on the impermeable boundaries must be calculated to ensure that the no-slip condition is satisfied there. This is achieved, and the vorticity function on the inflow boundary calculated, following Woods (1954), ensuring second-order accuracy. Conditions on the outflow boundary are implemented as in Roache (1972) to update both γ and ψ. With these updated boundary conditions equation (2.7)

is solved to give an updated approximation for ψ, and the process continued iteratively over the time step until successive iterates differ by less than a prescribed tolerance.

The presence of the singularity in the vorticity ζ, and therefore in the vorticity function γ, at $r = R_0$, $x = X_1$, that is, the convex corner of the bounding wall, invalidates the centred finite-difference representations of $\partial\gamma/\partial r$ at the point $(r_I - \delta r, x_J)$ and $\partial\gamma/\partial x$ at $(r_I, x_J + \delta x)$. In order to determine the values of γ at these two grid points we employ a local polar coordinate solution with origin at (r_I, x_J) and update the values each time the boundary values of γ are updated.

We assume that the flow is locally two-dimensional and use the results of Moffatt (1964). Sufficiently close to the corner inertial forces are negligible and for steady-state flow the stream function satisfies Stokes equation $\nabla^4\psi = 0$. We seek a solution near the corner of the form

$$\psi + \int_0^{R_0} s w_0(s, t)\,\mathrm{d}s = \sum_{i=1}^{\infty} \rho^{\lambda_i} F_i(t)\, G_i(\phi), \tag{3.1}$$

where (ρ, ϕ) are polar coordinates centred on (r_I, x_J), $\lambda_1 < \lambda_2 < \ldots$ are unknown constants and $F_i(t)$ and $G_i(\phi)$ are unknown functions of t and ϕ. This is the form of the solution for steady flow with functions of time $F_i(t)$ replacing constants. It is appropriate for unsteady flow provided that the Reynolds number is not large compared to ρ^{-2}. Substituting the expansion (3.1) for the stream function into the Stokes equation and solving subject to the no-slip conditions on the solid boundaries $\phi = -\frac{3}{4}\pi$, $\frac{3}{4}\pi$ gives for the first two terms of (3.1)

$$\psi + \int_0^{R_0} s w_0(s, t)\,\mathrm{d}s \sim A^*(t)\,\rho^{\lambda_1}\left\{\cos\lambda_1\phi - \frac{\cos\lambda_1\alpha}{\cos(\lambda_1 - 2)\alpha}\cos(\lambda_1 - 2)\phi\right\} + B^*(t)\,\rho^{\lambda_2}\left\{\sin\lambda_2\phi - \frac{\sin\lambda_2\alpha}{\sin(\lambda_2 - 2)\alpha}\sin(\lambda_2 - 2)\phi\right\},$$

where $\lambda_1 = 1.5445$, $\lambda_2 = 1.9085$, $\alpha = \frac{3}{4}\pi$, and $A^*(t)$, $B^*(t)$ are unknown functions. Therefore

$$-\frac{\gamma}{r} = \zeta \sim D^*(t)\,\rho^{\lambda_1 - 2}\cos(\lambda_1 - 2)\phi + E^*(t)\,\rho^{\lambda_2 - 2}\sin(\lambda_2 - 2)\phi, \tag{3.2}$$

where

$$D^*(t) = 4A^*(t)(1 - \lambda_1)\cos\lambda_1\alpha/\cos(\lambda_1 - 2)\alpha,$$

and

$$E^*(t) = 4B^*(t)(1 - \lambda_2)\sin\lambda_2\alpha/\sin(\lambda_2 - 2)\alpha.$$

The two functions $D^*(t)$, $E^*(t)$ are updated during every iteration, at each time level, from the values of γ at $(r_I + \delta r, x_J)$, $(r_I, x_J - \delta x)$. These updated values are then employed in equation (3.2) to determine the values of the vorticity function at $(r_I - \delta r, x_J)$ and $(r_I, x_J + \delta x)$.

The method is easily extended to model axisymmetric flow due to fluid motion through an annular orifice. Conditions for the solid boundaries $r = R_i$, $0 \leqslant x \leqslant X_1$ and $x = X_1$, $0 \leqslant r \leqslant R_i$ must be introduced, together with a treatment for the singular behaviour at the corner (R_i, X_1).

4. Results

We consider first the formation and development of a single vortex ring. We take the radius of the orifice in the plane boundary, $x = 0.2$, as $R_0 = 0.25$. The flow is initiated at $x = 0$ where we introduce the axial velocity profile

$$w_0(r, t) = f(r)\,g(t), \tag{4.1}$$

where

$$f(r) = \{1 - \mathrm{e}^{70(r - R_0)}\}. \tag{4.2}$$

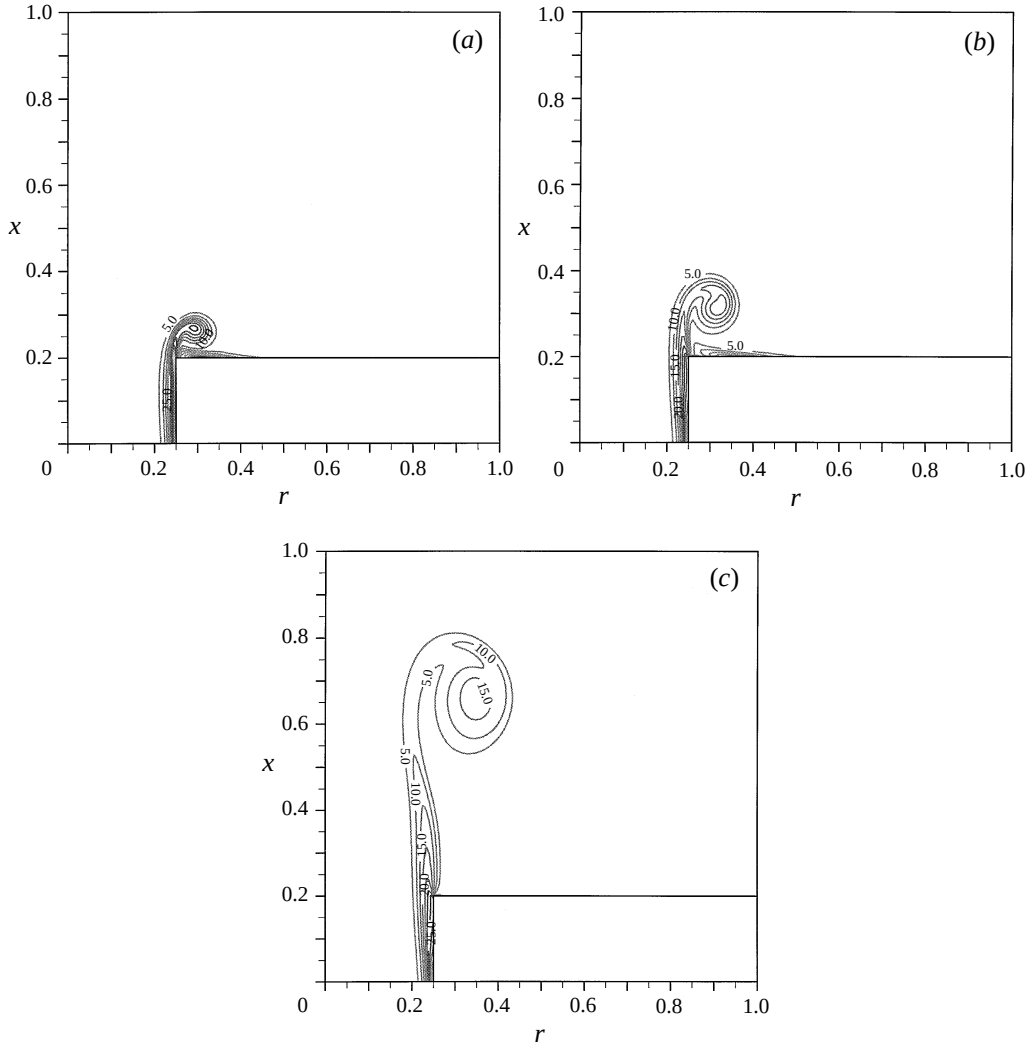

FIGURE 2. Contours of uniform vorticity during the formation of a single vortex ring, with an inlet flow (4.1) ($t_0 = 2$, $\bar{I} = 1.250$, $Re = 2000$, $g(t) = 1 - e^{-5t^2}$) at times (*a*) $t = 0.7$, (*b*) $t = 1.0$, (*c*) $t = 2.0$.

This corresponds to an inlet profile which has an almost uniform core flanked by thin boundary layers. For $g(t)$ we ensure that as $t \to 0$, $g(t) = O(t^2)$, to eliminate the singular behaviour that would be present at solid boundaries with, for example, an impulsive inlet profile. An important parameter that characterizes the flow is the impulse I' which, in dimensionless form, we define as

$$\bar{I} = \frac{I'}{\pi \rho R_0^2 \Gamma_0} = \frac{2}{R_0^2} \int_0^{t_0} \mathrm{d}t \int_0^{R_0} r w_0^2 \, \mathrm{d}r, \tag{4.3}$$

where t_0 is the time at which the inflow ceases.

For our first example we take $Re = 2000$, $g(t) = 1 - e^{-5t^2}$ and $t_0 = 2$ which gives $\bar{I} = 1.250$; and for all of our single-ring calculations we take $\delta t = \delta r = \delta x = 5 \times 10^{-3}$, and $X_0 = 4$. In all the cases considered we have checked the accuracy of our calculations by halving the temporal and spatial mesh size, at the same time reducing X_0 by a factor of two, and comparing the solutions over the initial formation period. The agreement

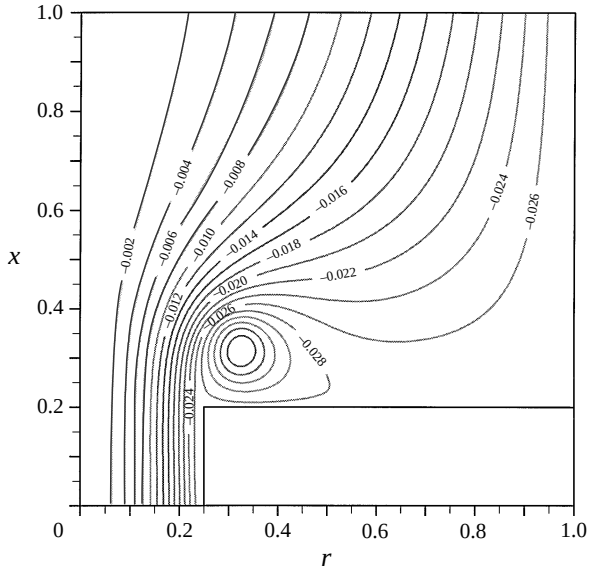

FIGURE 3. Streamline pattern corresponding to figure 2(*b*).

recorded confirms the accuracy of the solutions presented below. In figure 2 we show the early stages of ring formation. At $t = 0.7$, figure 2(*a*), the ring has clearly formed at the lip of the orifice, and by $t = 1.0$ is moving away under its own self-induced velocity, figure 2(*b*). Note that the circulation about the newly formed ring creates a thin boundary layer on $x = 0.2$, $r \geqslant 0.25$. Within this boundary layer the vorticity, ζ_b, is initially comparable with that in the core, ζ_c. For example at $t = 0.7$, $\max|\zeta_c| = 36.6$, $\max|\zeta_b| = 41.8$ and at $t = 1.0$, $\max|\zeta_c| = 28.9$, $\max|\zeta_b| = 27.0$. Thereafter the boundary-layer vorticity rapidly decays. Pullin (1979) has developed a similarity theory for the initial stages of ring formation from tube and orifice openings, created by a piston that moves with speed t^m. The theory is applied to the flow from a tube, and an orifice in an infinite flat plate. It is based on the idea that the vortex ring during formation is embedded within a potential flow, which is known exactly for the orifice in a thin plate, and has been calculated numerically by Pullin for the tube. In figure 3 we show the streamline pattern for the case under consideration here, at $t = 1.0$, which may be compared with the corresponding vorticity distribution in figure 2(*b*). It is clear that the ring is indeed forming in an initial potential flow, and that the boundary layer induced on the surface is of little dynamical significance. Pullin also considers the core structure within his similarity framework, and identifies three distinct regions. These are: (I) a tightly wound spiral-like thin shear layer from the forming edge, (II) an essentially inviscid rotational core, and (III) a viscous subcore. For the present example, if the vorticity contours $\zeta = 2.5, 17.5$ are taken to be representative of regions (II) and (III) respectively then we find, over the range $0.7 \leqslant t \leqslant 1.0$, that $r_{\mathrm{I}} \approx 0.1t^{2.23}$, $r_{\mathrm{II}} \approx 0.07t^{0.98}$, $r_{\mathrm{III}} \approx 0.03t^{0.44}$. The time-dependence $g(t)$ adopted here is not appropriate for the similarity theory. However, $g \approx 5t^2$ for $t \ll 1$, and applying the similarity theory with $m = 2$ gives the time-dependence for the scale of the three regions as $t^{2.25}$, $t^{1.04}$, $t^{0.5}$ respectively. As the ring continues to move away from the orifice, the boundary layer it induces on the plate dies away, until at $t = t_0 = 2$ it is virtually eliminated as we can see in figure 2(*c*). For $t > 2$ the vortex ring is free to detach itself completely from the orifice, and move away with its own self-induced velocity. The process by which this takes place is of interest. Immediately the inlet flow ceases a

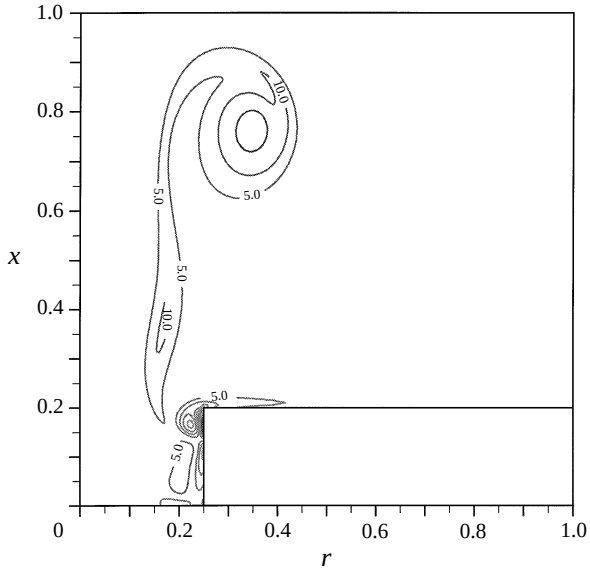

FIGURE 4. As figure 2 with $t = 2.3$.

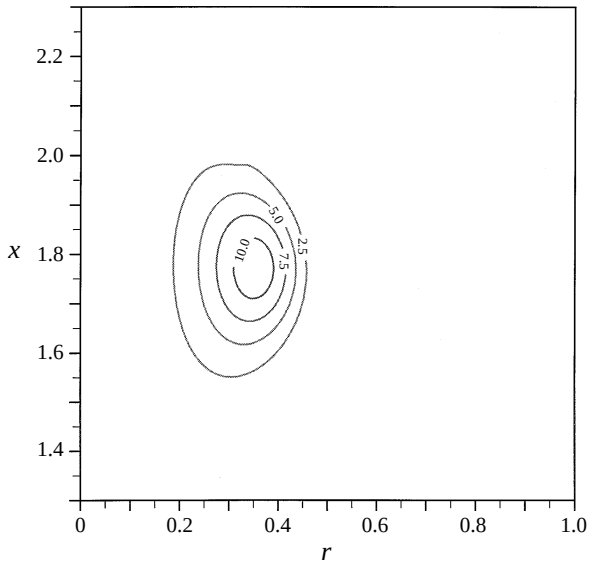

FIGURE 5. As figure 2 with $t = 5.0$.

vortex ring of opposite sign to the primary ring is formed at the lip of the orifice. This secondary ring begins to move back into the inlet tube $x < 0.2$, and at the same time draws back some of the vorticity previously shed in $t < 2.0$. This situation is well illustrated at $t = 2.3$ in figure 4. The primary vortex is, meanwhile, continuing to absorb the shed vorticity, and it is by these two mechanisms that the 'umbilical cord' connecting the vortex ring and orifice lip, as seen for example in figure 2(*c*), gradually disappears. The process is largely complete by $t = 2.5$. Thereafter the ring becomes an independent coherent structure propagating at almost constant speed with little change in cross-section, as for example in figure 5 at $t = 5$. The trajectory of the vortex ring,

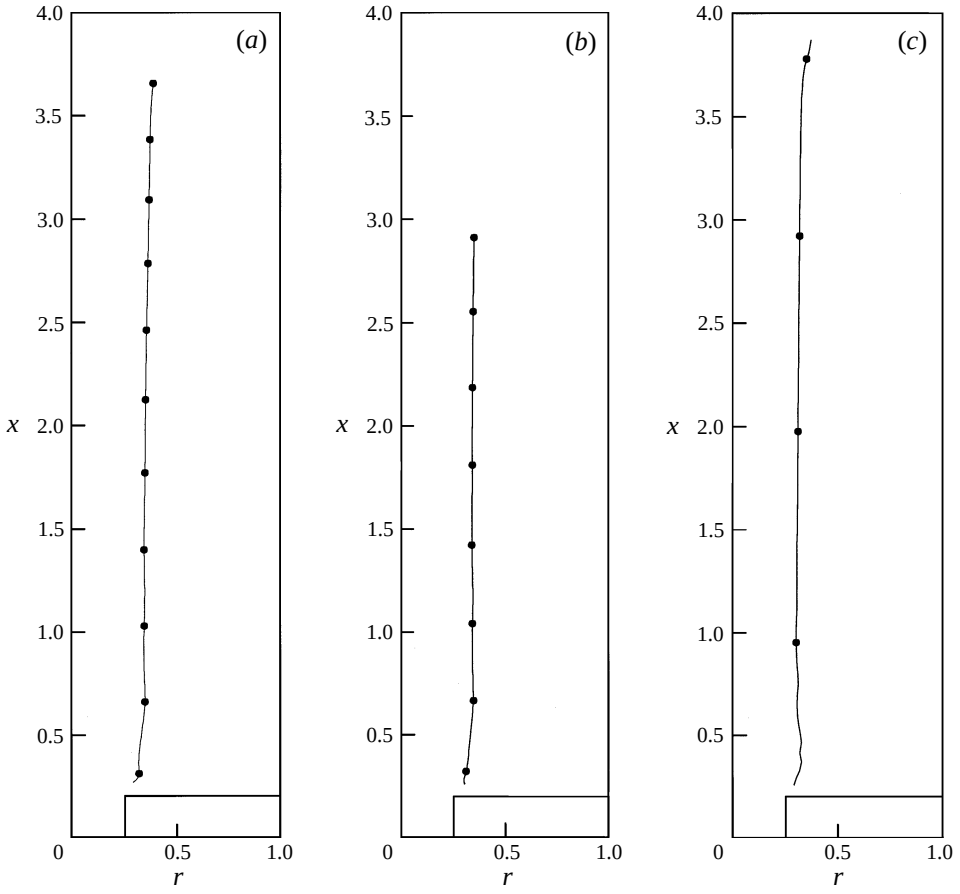

FIGURE 6. Trajectory of the vortex centre (*a*) for the case of figure 2: $t = 1.0$ (1.0) 11.0. (*b*) As (*a*) but with $Re = 4000$; $t = 1.0$ (1.0) 8.0. (*c*) For the case of figure 8; $t = 1.0$ (1.0) 4.0.

determined from the position of maximum vorticity, is shown in figure 6(*a*). Although this is difficult to locate at small time, the main features are well illustrated. For $0 \leqslant t \leqslant 2.0$ the ring increases in diameter; when the inlet flow ceases there is a slight reduction in ring diameter. The ring is now moving with almost constant speed, in fact gradually slowing as it again, gradually, increases in diameter. In figure 7 we show the shed circulation as a function of time. This is calculated from

$$\Gamma(t) = \int_S \zeta(r, x, t)\,\mathrm{d}x\,\mathrm{d}r, \tag{4.4}$$

where the domain of integration S is the region of flow in $x > 0.2$, chosen so that the thin boundary layer $0.2 \leqslant x \lesssim 0.2 + 2\delta x$, $r \geqslant 0.25$ is excluded. The shed circulation increases almost linearly for most of the formation period, reflecting the time-dependence, $g(t)$, of the inlet flow. When the inlet flow ceases, at $t = 2.0$, there is a sharp reduction in circulation for the reason advanced earlier, namely that previously shed circulation is drawn back into the inlet tube. The ring may be said to be fully formed at $t = 2.5$, at which time the circulation about the ring $\Gamma_r \approx 0.83$, so that the ring Reynolds number $\Gamma'/\nu = \Gamma_r Re \approx 1667$.

We have investigated a second example with these same inlet conditions, but with $Re = 4000$. The dynamics of formation and propagation are little different from those

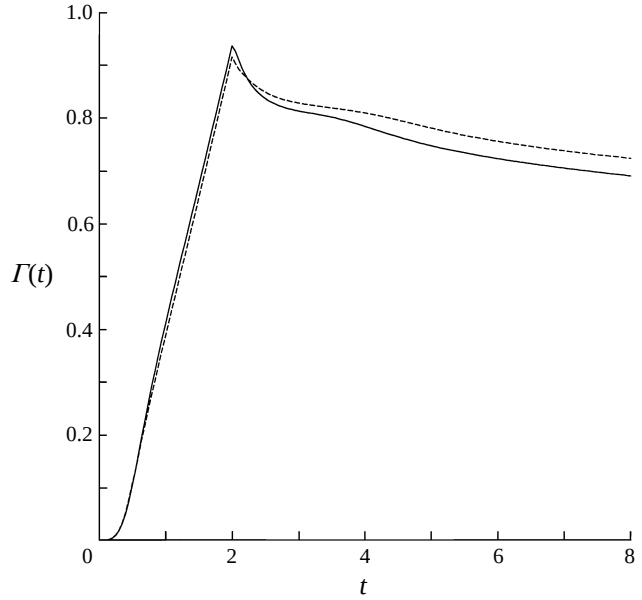

FIGURE 7. The shed circulation as a function of time for the case of figure 2 with $Re = 2000$ (——), and with $Re = 4000$ (----------).

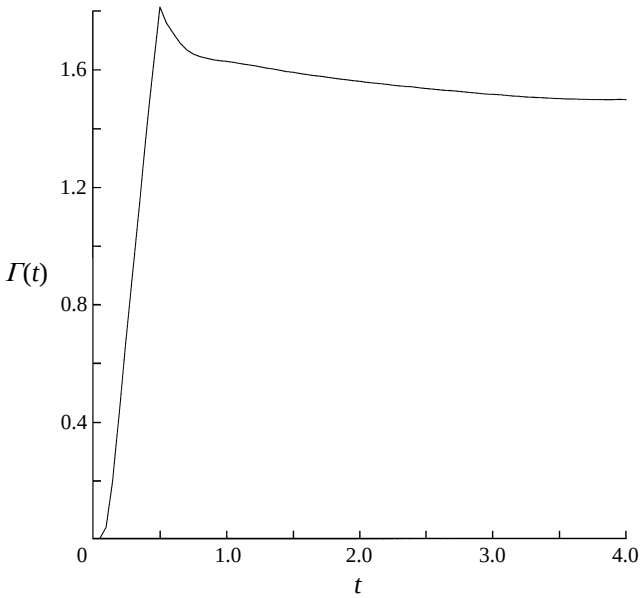

FIGURE 8. The shed circulation as a function of time for the configuration of figure 2, and inlet flow (4.1) ($t_0 = 0.5$, $\bar{I} = 2.410$, $Re = 2000$, $g(t) = 3(1-e^{-40t^2})$).

described above, as may be inferred from the shed circulation, and ring trajectory, shown in figures 7 and 6(*b*) respectively. There is only a weak dependence upon the Reynolds number, manifested for example in a slightly greater propagation speed, a point to which we shall return later.

In a final example we have taken $g(t) = 3(1-\mathrm{e}^{-40t^2})$, $t_0 = 0.5$, with corresponding impulse $\bar{I} = 2.410$, and $Re = 2000$. The processes by which the ring is formed are as

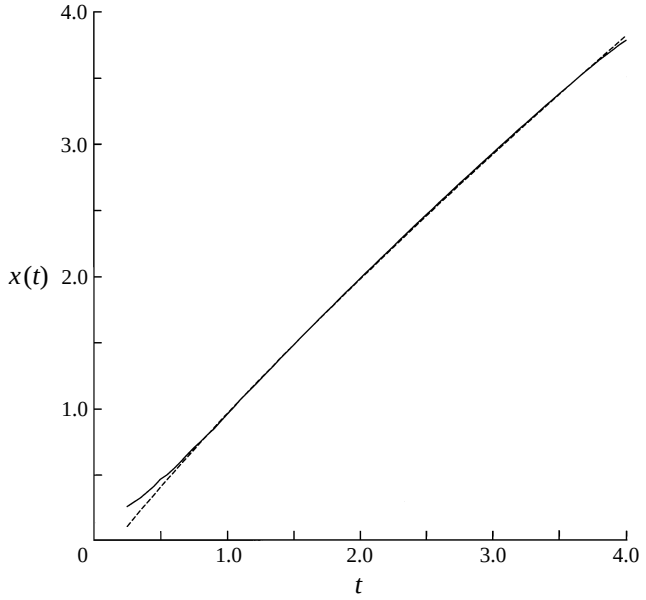

FIGURE 9. The progression of the vortex core for the case of figure 8 (——) compared with result (4.5) with $F = 4.103$ (----------).

described above. However, in this case circulation is shed at a much greater rate as we see in figure 8. When the inlet flow ceases we again note a sharp drop in circulation for the reasons advanced above. The ring, when fully formed at $t = 1$, say, has circulation $\Gamma_r \approx 1.68$ which leads to a ring Reynolds number $\Gamma_r Re \approx 3360$. The ring formed by this greater impulse propagates more rapidly as we see from the trajectory in figure 6(*c*). Also, as we may expect, it results in a ring that is more compact, or of smaller cross-sectional area. For rings of small circular cross-section Saffman (1970) has estimated the velocity of viscous vortex rings. In particular, if the circulation can be expressed in the form $\Gamma = \Gamma(s/t^{1/2})$, where s is a radial coordinate measured from the centre of the cross-section, then the ring velocity w_r takes the form

$$w_r = \frac{1}{4\pi R}\{F(Re_r, R) - \tfrac{1}{2}\ln t + \ldots\}. \tag{4.5}$$

In (4.5) R is the ring radius, and $Re_r = \Gamma_r'/\nu$ is the ring Reynolds number upon which F depends only weakly; for example, with a distribution of Γ as in Lamb's vortex we have $F = 0.828 + \frac{1}{2}\ln R^2 Re_r$. For the example under consideration our ring has radius $R = 0.304$ and a relatively small, almost circular, cross-section. If we set $F = 4.103$ then there is close agreement between (4.5) and our calculated values of w_r, as shown in figure 9 for $1 \leqslant t \leqslant 3.5$, beyond which the presence of the upper boundary influences the flow. Furthermore the acceleration of the ring is indistinguishable from the result $\mathrm{d}w_r/\mathrm{d}t = -(8\pi Rt)^{-1}$, which is Reynolds-number independent. These results both substantiate our earlier comment about the weak dependence of the flow upon Reynolds number, and demonstrate the robustness of Saffman's theory.

The above discussion shows that when the fully formed ring is moving freely, the dynamics are largely inviscid in nature. This invites a comparison with inviscid theory. Inviscid vortex rings have been considered by Norbury (1973), in which the vorticity increases linearly across the core of the vortex ring. It is of interest to compare, in this

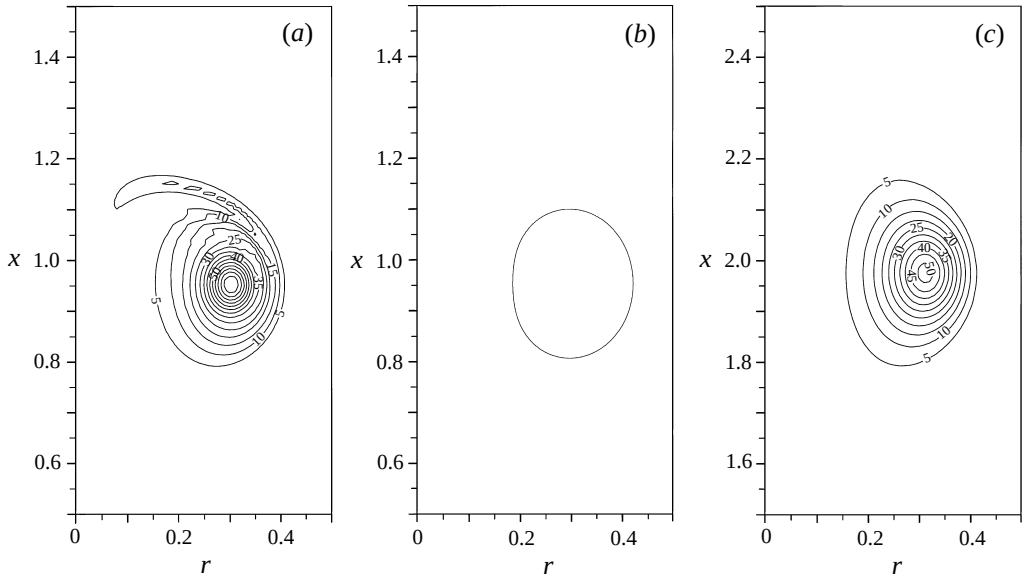

FIGURE 10. Contours of uniform vorticity for the case of figure 8 at (*a*) $t = 1.0$, (*c*) $t = 2.0$, and (*b*) a cross-section of the core of the equivalent Norbury ring.

present example, our ring with an 'equivalent' Norbury ring. In figure 10(*a*) we show the cross-section of our virtually fully formed ring at $t = 1.0$. In figure 10(*b*) we show, in cross-section, the equivalent Norbury ring, designed to have the same speed, radius, and circulation at this instant. In figure 10(*c*) we reproduce our viscous ring at $t = 2.0$. The similarity of these is evident. This not only confirms the largely inviscid nature of the flow when the ring is fully formed, but also suggests that the detailed distribution of vorticity in the core of the ring is relatively unimportant in determining its dynamics.

We turn our attention next to the formation and propagation of coaxial pairs of vortex rings, including the vortex-ring pair. The latter is a configuration first investigated by Weidman & Riley (1993), defined as a coaxial pair that propagates in a coherent, coplanar manner. The investigation of Weidman & Riley included both experiment and numerical simulation. In the experiments pairs of vortex rings were formed by the impulsive motion of liquid, provided by the motion of a manually activated piston, through an annular circular orifice. Vortex rings of opposite circulation are formed at the lip of the orifice. Their subsequent behaviour depends upon the relative strength of the circulation about the rings. Assuming that the rings remain stable and coaxial, their motion may be explained as follows. As we have seen above, a single ring created at the outer edge of the annulus would be self-propelled away from it. The mutual interaction between two rings, formed as described above, acts to push them both in this same direction. However, the self-induced velocity of the inner ring is in the opposite direction. If it were sufficiently strong then one might suppose it would separate from the outer ring and propagate back to its point of origin, whilst if it were sufficiently weak one might expect that it would be pushed through, and ahead, of the outer ring. These alternatives suggest a particular balance that would result in the vortex-ring pair. Of course, a truly steady vortex-ring pair can never be fully realized, owing to the continuous redistribution of vorticity by viscous diffusion. Nevertheless, the experiments did show that quasi-steadily propagating vortex-ring pairs are a viable proposition, if only over relatively short distances before ultimate decay or destruction by instability. The simulation of these flows carried out by

Weidman & Riley was in two parts. An inviscid thin-ring theory readily yielded the vortex-ring pair. But most effort was expended on Navier–Stokes calculations. The approach was as follows. No attempt was made there to simulate vortex-ring formation. Instead the initial configuration had each ring represented by the viscous line vortex solution of Lamb (1932). An exhaustive investigation, continued by Riley (1993), was carried out for different orifice gap widths with the rings initially co-planar at a finite time. And it was shown *inter alia* that a vortex-ring pair, as discussed above, could be formed. To simulate the experiments these vortex rings were placed at the location of the observed rings, at the time when the piston motion ceased. By judiciously choosing the circulation ratio of the two rings, excellent agreement with the observed ring trajectories was obtained.

In our present study we do not attempt an accurate simulation of the experiments of Weidman & Riley, on account of the complex configuration of their vortex-ring generator. We adopt instead the simpler geometry of figure 1 in which an inner cylinder is placed in the tube from which fluid is forced, to create an annular gap in the plane of $x = 0.2$. In these calculations the outer radius of the annulus was taken as $R_0 = 0.5$, and the outer boundary as $X_0 = 3$, which is less than for the single-ring calculations since more computer time is required for these flows of greater complexity. The computational mesh size was taken to be the same as for the single-ring calculations with the Reynolds number $Re = 2000$ which is comparable with those of the experiments. For the inlet flow we take $t_0 = 0.3$, and

$$w_0 = \lambda(1-\mathrm{e}^{-500t^2})\{1-\mathrm{e}^{15000(r-R_i)\,(r-R_0)}\}, \tag{4.6}$$

where R_i is the inner radius of the annulus.

Weidman & Riley identify the annular gap width, or radius ratio $\delta = R_i/R_0$, and the impulse $\bar{I}$, in which the orifice area $A_0 = \pi(R_0^2 - R_i^2)$ is now taken as the characteristic area, as the key parameters that determine the nature of the flow following the formation of the rings. As we have already remarked it is not our intention to accurately simulate the experiments of Weidman & Riley. Our aim is to demonstrate that the various scenarios observed in their experiments can be reproduced from our simpler configuration. The formation process for the two rings is similar to that described for the single ring. However, we do note that for $t > t_0$ we now have a secondary pair of vortex rings forming at the orifice lips, as has been observed in the experiments.

In our presentation of results we concentrate largely on the vortex trajectories, as indeed did Weidman & Riley. In the experiments small blobs of dye provided a visual marker of the centre of the vortex-ring core sections. However, as we shall see later, such information reveals only partially the flow characteristics. Figure 11 shows the influence of gap width, or radius ratio δ, on the flow, although we note that the impulse $\bar{I}$ varies marginally in this set of results. In figure 11(*a*), for relatively small δ, the interaction between the rings is not significant. The inner ring penetrates only a short distance before separating and moving back with its own self-induced velocity. As the gap closes, figure 11(*b*), the penetration distance of the inner ring increases, due to the nearness of the outer ring, before it again separates and moves back. Closing the gap even further, and by only one mesh increment δr, brings about a dramatic change in the flow behaviour as we see in figure 11(*c*). The mutual interaction between the rings now results in the inner ring being pushed slightly ahead of the outer. As soon as this happens the interaction leads to an increase in the diameter of both rings, with the result shown in the figure. With a further increase in δ, figure 11(*d*), this process is accelerated. We may anticipate that a situation will exist, between those shown in

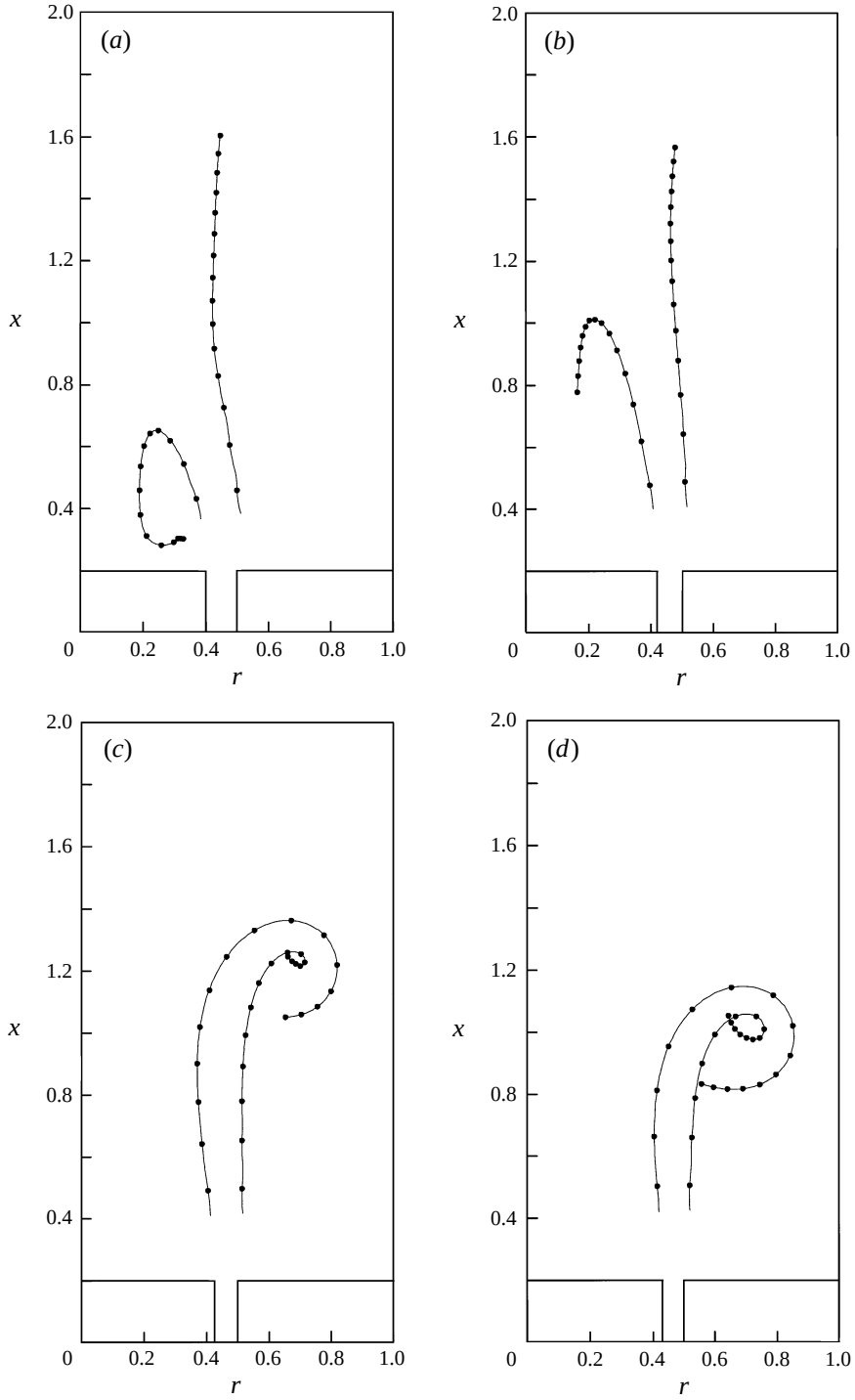

FIGURE 11. Vortex-ring trajectories, $t = 0.5$ (0.25) 4.0, for the pairs formed with inlet flow (4.6), $R_0 = 0.5, \lambda = 2.0$, and with $Re = 2000$. (*a*) $R_i = 0.4, \bar{I} = 0.975$; (*b*) $R_i = 0.42, \bar{I} = 0.963$; (*c*) $R_i = 0.425, \bar{I} = 0.959$; (*d*) $R_i = 0.43, \bar{I} = 0.953$.

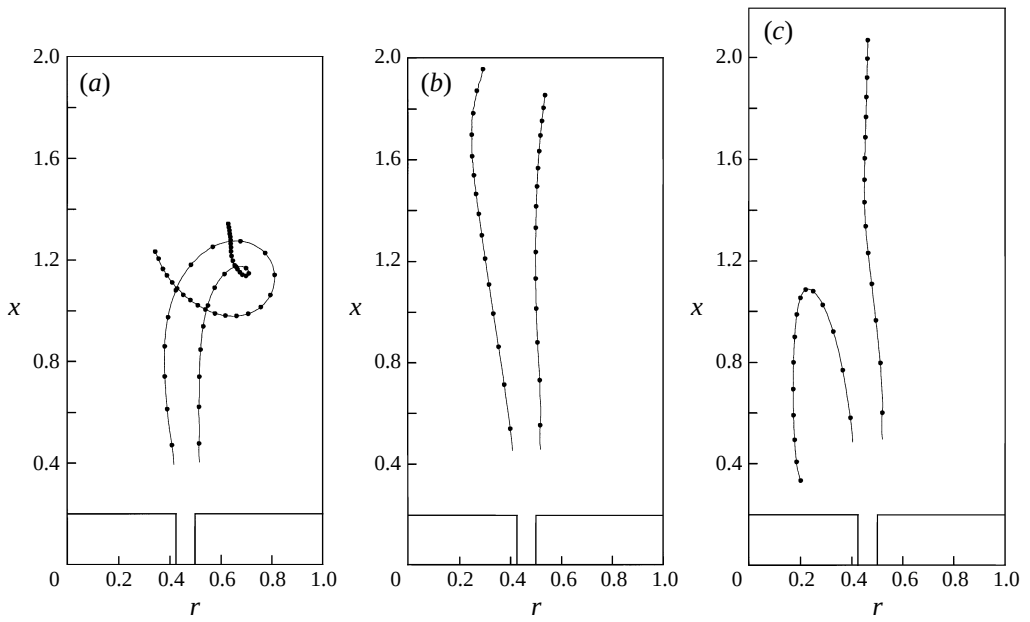

FIGURE 12. Vortex-ring trajectories, for the pairs formed with inlet flow (4.6), $R_0 = 0.5$, $R_i = 0.425$, and with $Re = 2000$, (*a*) $\lambda = 1.9$, $\bar{I} = 0.866$, $t = 0.5$ (0.25) 7.0; (*b*) $\lambda = 2.269$, $\bar{I} = 1.236$, $t = 0.5$ (0.25) 4.0; (*c*) $\lambda = 2.5$, $\bar{I} = 1.500$, $t = 0.5$ (0.25) 4.0.

figures 11(*b*) and 11(*c*), that corresponds to a vortex-ring pair. The results of figure 11 are consistent with those shown in figure 15 of Weidman & Riley, namely that a transition from the return, or separation, of the inner ring, to no return, takes place as δ increases. We next consider the effect of the impulse $\bar{I}$. For this we fix $R_i = 0.425$, so that $\delta = 0.85$ and $\bar{I} = 0.240\,\lambda^2$. The results are shown in figure 12. There we see a transition from no return to separation, and return, as λ increases from 1.9 to 2.5. This again is consistent with the results of Weidman & Riley. At an intermediate value, $\lambda = 2.269$, shown in figure 12(*b*), we see an example of a vortex-ring pair, in the sense of Weidman & Riley (1993) and Riley (1993) who have used that term for a coherent structure seen, or calculated, to propagate an axial distance R_0 and 2.5 R_0, respectively. However, as we have already remarked neither the vortex trajectories nor other details reported from the flow visualizations reveal much of the structure of the flow. In figure 13 we present the vorticity field for each of the cases shown in figure 12. We note that in each case there is already a distinct difference in the shape of the ring cross-sections at $t = 0.5$. This reflects, in part anyway, the difference in the strengths of each ring. If the extrema ζ_{max}, ζ_{min} are taken as a measure of the strengths of the outer and inner rings, then for each of the cases shown $\max|\zeta_{min}/\zeta_{max}|$ lies in the range 0.85 to 0.9. In the subsequent motion we see that as long as the two rings remain in close proximity the action of the stronger, outer ring is to 'strip' vorticity from the inner and so elongate it. Simultaneously the inner ring is rapidly decaying due to diffusion. These effects are most prominent in figure 13(*a*) where the close interaction between the rings is most persistent. There we see that the effects of diffusion have also resulted in a significant weakening of the outer ring. This case may be contrasted with that shown in figure 13(*c*). There the rapid separation of the two rings leaves each of them relatively intact. There is a considerable reduction in the vorticity of the inner ring in this case, of course, as it shrinks in diameter.

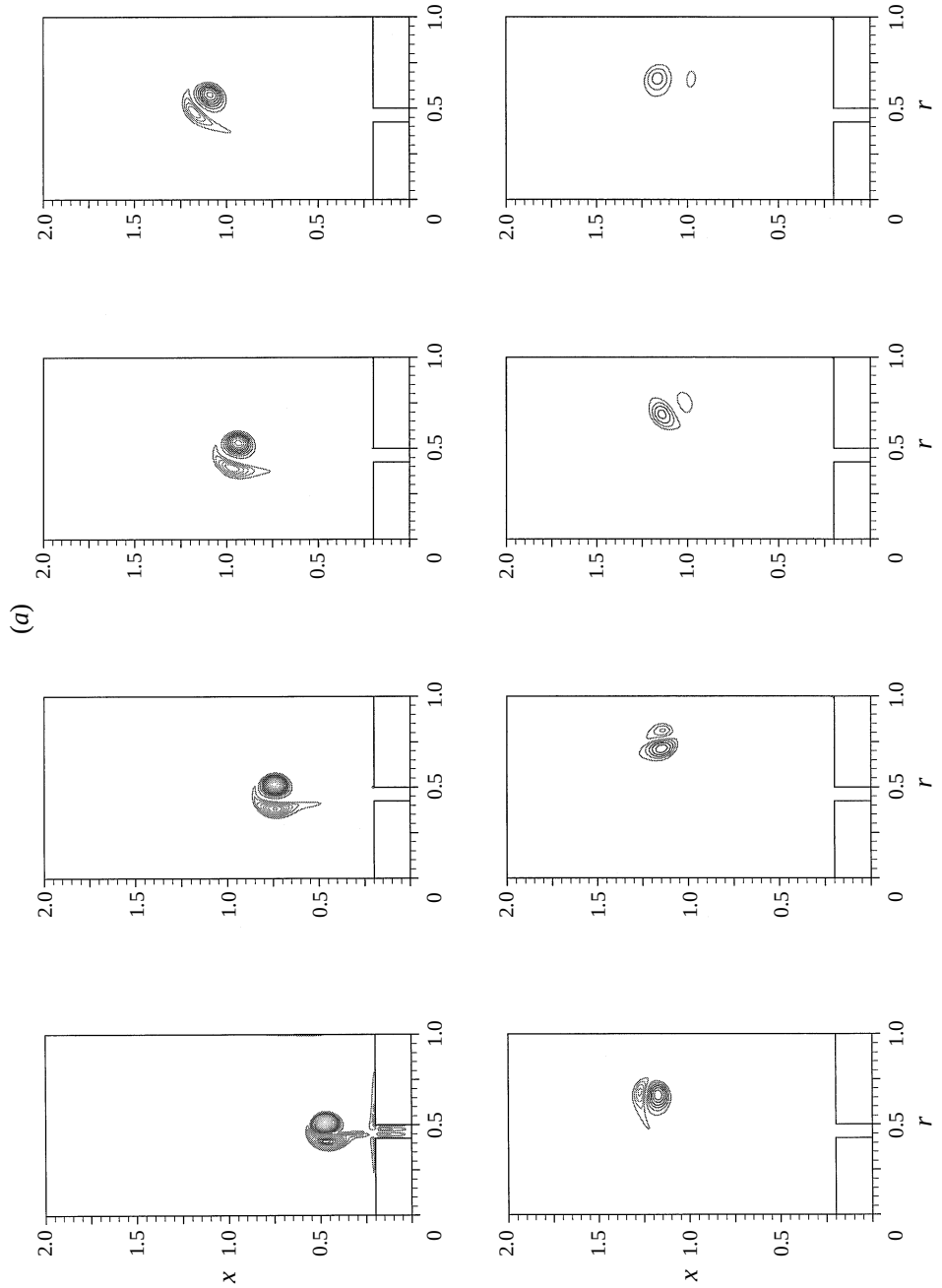

FIGURE 13(*a*). For caption see page 138.

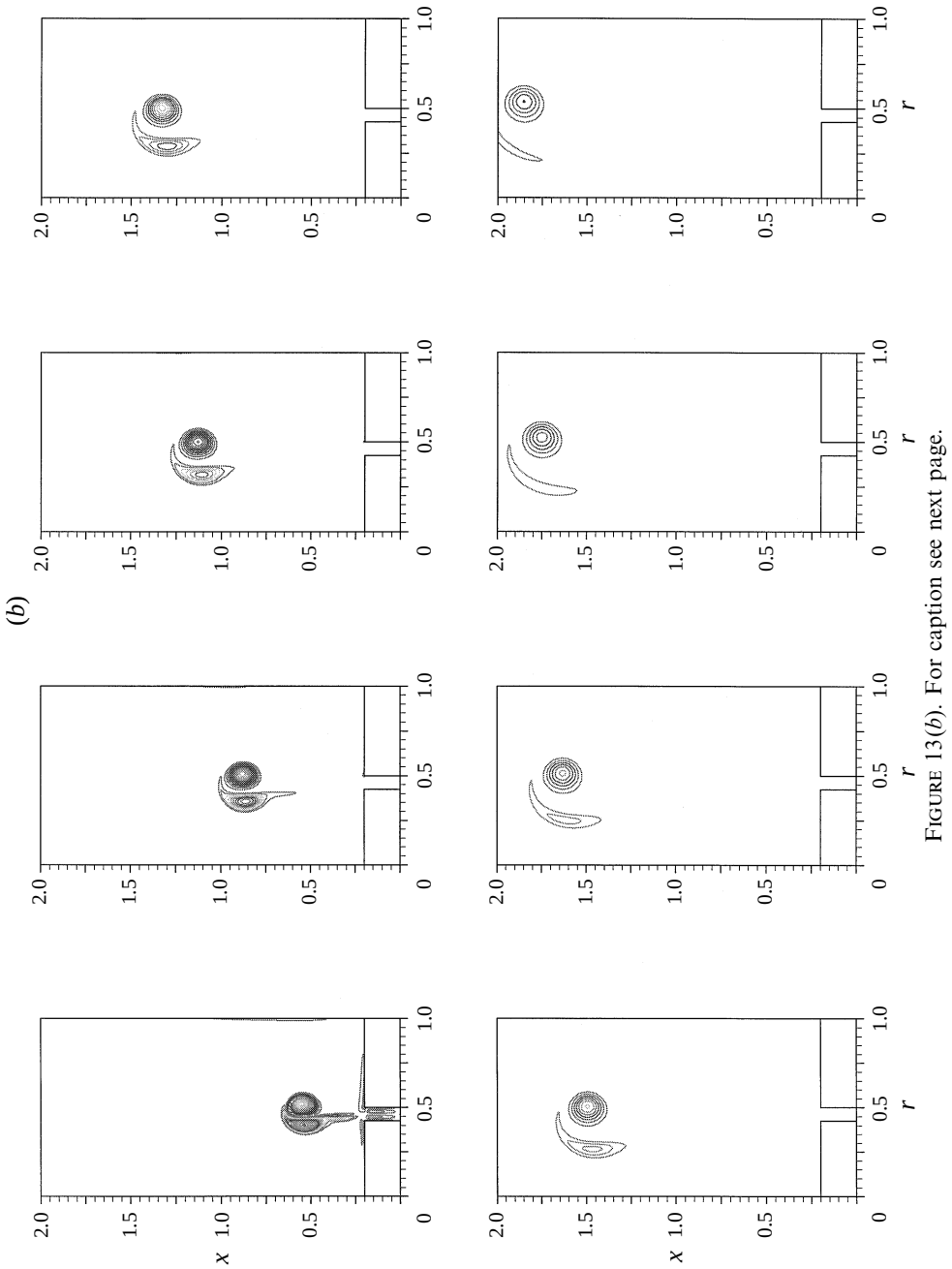

FIGURE 13(*b*). For caption see next page.

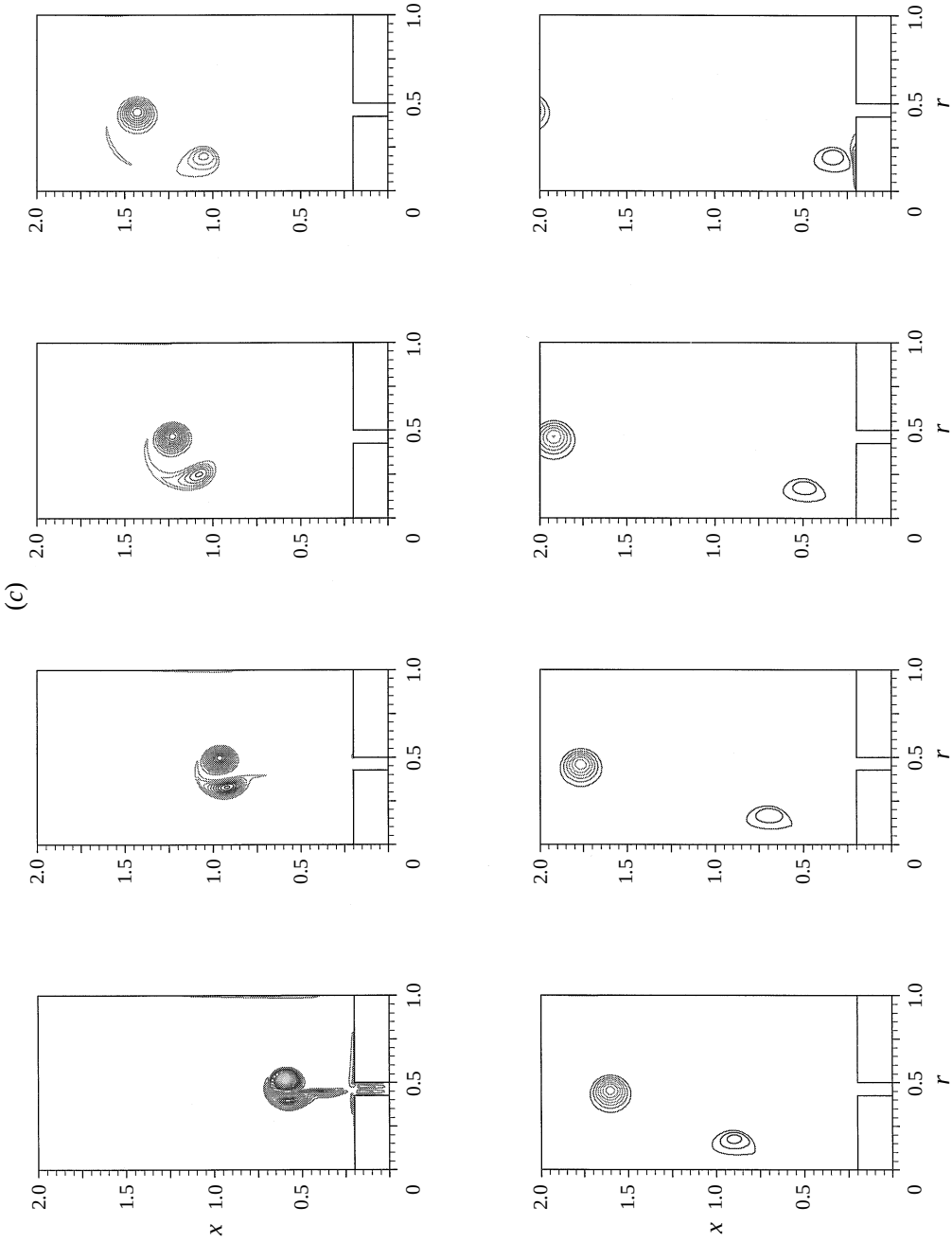

FIGURE 13. Contours of uniform vorticity, corresponding to the cases of figure 12, with $\min|\xi| = 5.0$ and neighbouring contours at intervals 5.0 (outer ring), -5.0 (inner ring), $t = 0.5$ (0.5) 4.0.

Although in many of the cases considered the inner ring is ultimately a feeble feature, when compared with the outer, it is still possible to identify ζ_{min} and create the trajectories shown in figures 11 and 12. Similarly, in the experiments of Weidman & Riley (1993) a small blob of dye trapped at the centre of the vortex-ring core enables identification of that ring to be maintained. However, the results we have described above show that the vortex trajectories themselves reveal little of the true flow structure. We believe that our investigation has provided a much deeper insight into the behaviour of flows associated with pairs of vortex rings of the kind first realized by Weidman & Riley. In particular, with reference to the numerical simulations therein, extended by Riley (1993), we comment as follows. The use of very thin viscous vortex rings as an initial condition is helpful in delineating the wide variety of behaviour that may be expected. However, it is very clear from figure 13 that such an initial configuration, where the two rings are typically distinct, cannot be a good representation of the 'cheek-by-jowl' situations that are typical of the initial formation process as seen in figure 13.

During the course of this work financial support for S.L.W. was provided by an EPSRC research grant.

REFERENCES

Lamb, H. 1932 *Hydrodynamics*. Cambridge University Press.

Moffatt, H. K. 1964 Viscous and resistive eddies near a sharp corner. *J. Fluid Mech.* **18**, 1–18.

Norbury, J. 1973 A family of steady vortex rings. *J. Fluid Mech.* **57**, 417–431.

Pullin, D. I. 1979 Vortex ring formation at tube and orifice openings. *Phys. Fluids* **22**, 401–403.

Riley, N. 1993 On the behaviour of pairs of vortex rings. *Q. J. Mech. Appl. Maths* **46**, 521–539.

Roache, P. J. 1972 *Computational Fluid Dynamics*, chap. III-C-6. Hermosa.

Saffman, P. G. 1970 The velocity of viscous vortex rings. *Stud. Appl. Maths* **49**, 371–380.

Wakelin, S. L. & Riley, N. 1996 Vortex ring interactions II. Inviscid models. *Q. J. Mech. Appl. Maths* **49**, 287–309.

Weidman, P. D. & Riley, N. 1993 Vortex ring pairs: numerical simulation and experiment. *J. Fluid Mech.* **257**, 311–337.

Woods, L. C. 1954 A note on the numerical solution of fourth order differential equations. *Aero. Q.* **5**, 176–182.